Natural variation in ENSO flavors

Matthew Newman,[1,2] Sang-Ik Shin,[3] and Michael A. Alexander[2]

Received 2 April 2011; revised 16 May 2011; accepted 18 May 2011; published 27 July 2011.

[1] Using a multivariate, "patterns-based", red noise approach to 42 years of observed tropical SST, thermocline depth, and zonal wind stress seasonal anomalies, it is shown that natural random variations can account for the observed variability of Central Pacific (CP) and Eastern Pacific (EP) ENSO events. The recent multidecadal increase in the number of CP events relative to EP events, which has been hypothesized to be connected to anthropogenic change in the state of the ocean, is also found to be consistent with multivariate red noise and hence with stationary statistics. ENSO "flavors" are the consequence of differing combinations of two initially orthogonal spatial patterns that are precursors to CP or EP events of both signs. These precursors can be excited by random weather forcing and subsequently result in SST anomaly amplification primarily through surface or thermocline feedbacks, respectively. **Citation:** Newman, M., S.-I. Shin, and M. A. Alexander (2011), Natural variation in ENSO flavors, *Geophys. Res. Lett.*, *38*, L14705, doi:10.1029/2011GL047658.

1. Introduction

[2] El Niño-Southern oscillation (ENSO), the dominant tropical coupled atmosphere-ocean phenomenon on interannual time scales, impacts the climate not only over the tropics but also over the globe [e.g., *Alexander et al.*, 2002]. Historically, El Niño has been defined as the appearance of warm sea surface temperature (SST) anomalies in the eastern tropical Pacific including the "Niño3" region (5°S–5°N and 150°W–90°W). However, some El Niño events, particularly recently, have maximum SST anomalies located primarily in the central tropical Pacific "Niño4" region (5°S–5°N and 160°E–150°W), with attendant shifts in both atmospheric teleconnections and their worldwide impacts compared to the canonical ENSO [e.g., *Ashok et al.*, 2007; *Kim et al.*, 2009; *Yeh et al.*, 2009; *Di Lorenzo et al.*, 2010; *Mo*, 2010; *Yu and Kim*, 2011].

[3] It has long been recognized that each El Niño event may have differences in detail from the standard composite during the course of its evolution; this has sometimes been referred to as different ENSO "flavors" and can be represented, for example, by secondary ENSO indices representing east-west SST differences [e.g., *Trenberth and Stepaniak*, 2001]. This diverse El Niño evolution received much attention recently after *Yeh et al.*'s [2009] analysis of El Niño in the IPCC AR4 future climate projections suggested that increasing "CP-El Niño" occurrence could be a response to ongoing greenhouse warming. In their nomenclature, an EP-El Niño (CP-El Niño) event occurs when the Niño3 (Niño4) SST anomaly is greater than 0.5°C and greater than the Niño4 (Niño3) anomaly. Observational studies suggesting that CP-El Niño has increasingly become the dominant form of El Niño since the late 1960s have also raised the possibility that some natural and/or anthropogenic "base state" change (that is, a substantial difference in the ocean mean state that alters stability properties) has changed characteristic El Niño evolution [*Yeh et al.*, 2009; *Lee and McPhaden*, 2010]. On the other hand, using the 4200 year long Kiel Climate Model simulations, *Yeh et al.* [2011] showed that the frequency of CP-El Niño occurrence can increase without any changes in radiative forcings, and acknowledged that an increasing frequency of CP-El Niño occurrence may also be consistent with natural climate variability. However, considering the deficient simulations of El Niño in coupled climate models [*Guilyardi et al.*, 2009; *Newman et al.*, 2009; *Yu and Kim*, 2010], the latter conclusion may also be highly model dependent [see *Yeh et al.*, 2009, Figure 3].

[4] The questions raised by these studies can be summarized as: 1) does the recent increase in CP ENSOs reflect decadal base state change? and 2) does the recent increase in CP ENSOs reflect anthropogenic change? To answer these questions, it is important to first construct a suitable null hypothesis against which both observational and modeling studies may be tested: *observed changes in ENSO characteristics are consistent with natural seasonal variability with stationary statistics.* A standard null hypothesis in climate studies is to compare the variability of a time series, either of an index or of a value at a fixed location, to scalar "red noise". We suggest that when testing changing relationships between multiple indices, or more generally the variability of a series of evolving maps, the appropriate comparison is to multivariate red noise. In this paper, using statistically stationary multivariate red noise determined from observed tropical SST, thermocline depth, and zonal wind stress seasonal anomalies, we find the expected multidecadal range in the relative frequency and amplitude of CP and EP ENSO events and compare this range to what has so far been either observed or projected to occur.

2. "Patterns-Based" Multivariate Red Noise

[5] Climate variability is often characterized by a notable separation between the dominant time scales of interacting processes. For example, compared to the much longer timescales of the ocean, weather varies so rapidly that it can be considered to have almost no memory. Weather forcing of the oceanic mixed layer can then be approximated as white

[1]Climate Diagnostics Center, CIRES, University of Colorado at Boulder, Boulder, Colorado, USA.
[2]Physical Sciences Division, Earth System Research Laboratory, NOAA, Boulder, Colorado, USA.
[3]College of Marine Science, University of South Florida, St. Petersburg, Florida, USA.

0094-8276/11/2011GL047658

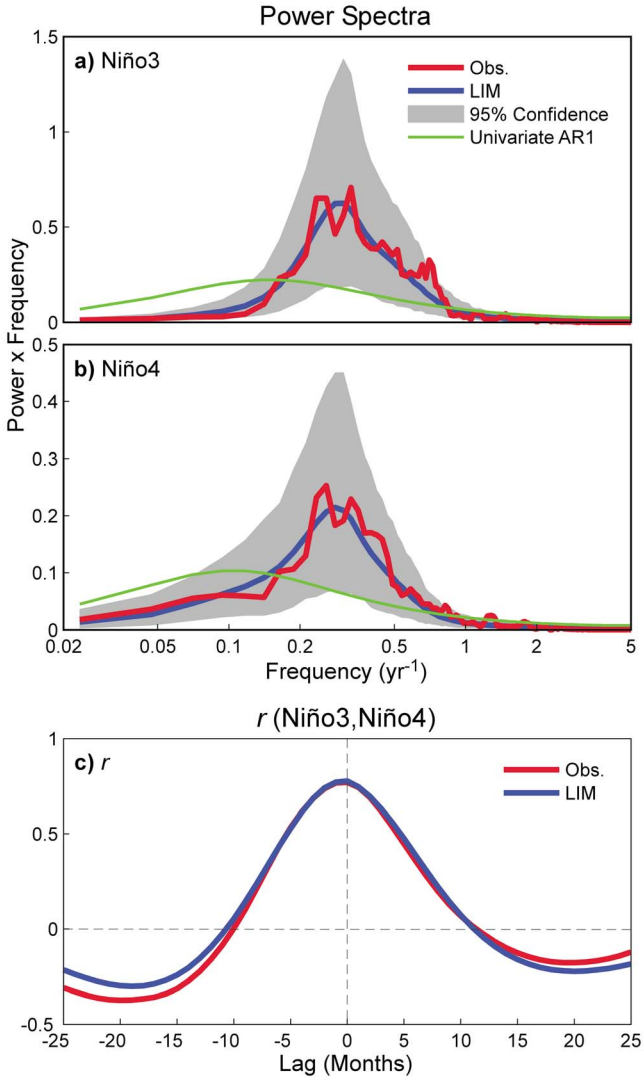

Figure 1. Power spectra for the (a) Niño 3 and (b) Niño4 SST indices for the years 1959–2000 (red lines), compared to those predicted by multivariate red noise (i.e., the LIM; blue lines) and by a univariate red noise fit (green lines). Gray shading represents the 95% confidence interval determined from a 500-member ensemble of 42 yr-long LIM forward integrations (see NAS for further details). In these log (frequency) versus power times angular frequency (ω) plots, the area under any portion of the curve is equal to the variance within that frequency band. Note that displaying power times frequency slightly shifts the power spectral density peak centered at a period of 4.5 yrs to a variance peak centered at a period of 3.5 yrs. (c) Correlation between Niño 3 and Niño 4 indices, for lags ranging up to 25 months. Positive lags indicate Niño 3 leads Niño 4; negative lags indicate Niño 4 leads Niño 3.

noise forcing of a damped integrator [e.g., *Hasselmann*, 1976]. This is an example of *univariate red noise* (also called an AR1 process) for an anomaly scalar time series $x(t)$, the simplest null hypothesis for both atmospheric and oceanic climate variability [e.g., *Wunsch*, 1999; *Rudnick and Davis*, 2003].

[6] When extended to the more general case of an anomaly state vector $\mathbf{x}(t)$ representing many evolving regional patterns of climate variables, this approximation based on time scale separation becomes *multivariate red noise*,

$$\frac{d\mathbf{x}}{dt} = \mathbf{L}\mathbf{x} + \xi \tag{1}$$

[e.g., *Penland and Sardeshmukh*, 1995], with two notable differences from univariate red noise. First, $\mathbf{L}$ is a two-dimensional damped linear operator representing both local and non-local dynamics, including interactions between variables, so multivariate red noise represents the evolution of both stationary and propagating anomaly patterns (i.e., eigenmodes of $\mathbf{L}$); scalar indices derived from $\mathbf{x}$ can then have spectral peaks [e.g., *Newman*, 2007]. Second, some characteristic physical processes operate mostly in one direction – for example, atmospheric wind stress directly drives ocean circulation and thermocline changes but not vice versa [e.g., *Moore and Kleeman*, 1999] – so $\mathbf{L}$ does not have symmetric dynamical relationships between all elements of $\mathbf{x}$. Consequently, despite the lack of exponential modal instability, some anomalies experience significant but transient growth over finite time intervals (i.e., $\mathbf{L}$ is stable but non-self adjoint [e.g., *Farrell*, 1988]), since anomalies that are initially best configured to grow also evolve into new patterns and/or move into new regions that lead to decay. These "optimal structures" [e.g., *Penland and Sardeshmukh*, 1995] are initiated by some realizations of the unpredictable white noise ξ, which has spatial but no temporal coherence.

[7] The empirical method that determines multivariate red noise from observations is Linear Inverse Modeling (LIM) [*Penland and Sardeshmukh*, 1995]. In this paper, we use the LIM developed by *Newman et al.* [2011, hereafter NAS], in which $\mathbf{x}$ consists of 3-month running mean anomalies of observed SST [*Rayner et al.*, 2003], thermocline depth (depth of 20°C isotherm) [*Carton and Giese*, 2008], and surface zonal wind stress [*Kalnay et al.*, 1996] in the Tropics (30°S–30°N) during 1959–2000. We integrated (1) forwards for 24000 yrs, treating it as a stochastically-forced dynamical model following NAS. Repeating our study using detrended data yielded negligible differences in all results reported below.

3. Distinguishing CP and EP Events Within Multivariate Red Noise

[8] NAS verified multivariate red noise with tests ensuring that when (1) is determined from a specified lag (here, 3 months) it accurately reproduces observed evolution statistics at much longer time scales. Here we verify that CP and EP ENSO variations are reproduced by multivariate red noise. First, Niño3 and Niño4 power spectra determined by (1) are compared to the observed spectra in Figure 1. The multivariate red noise and observed spectra closely match, with a strong peak in the 2–7 year band and small deviations that are not statistically significant. In contrast, the spectra of virtually all ensemble members of the "20th-century" (20c3m) IPCC AR4 coupled GCMs lie substantially outside the 95% confidence interval [not shown, but see *Newman et al.*, 2009]. Additionally, Figure 1c shows that the simultaneous and lagged correlation between Niño3 and Niño4, r(Niño3, Niño4), determined from (1) compares

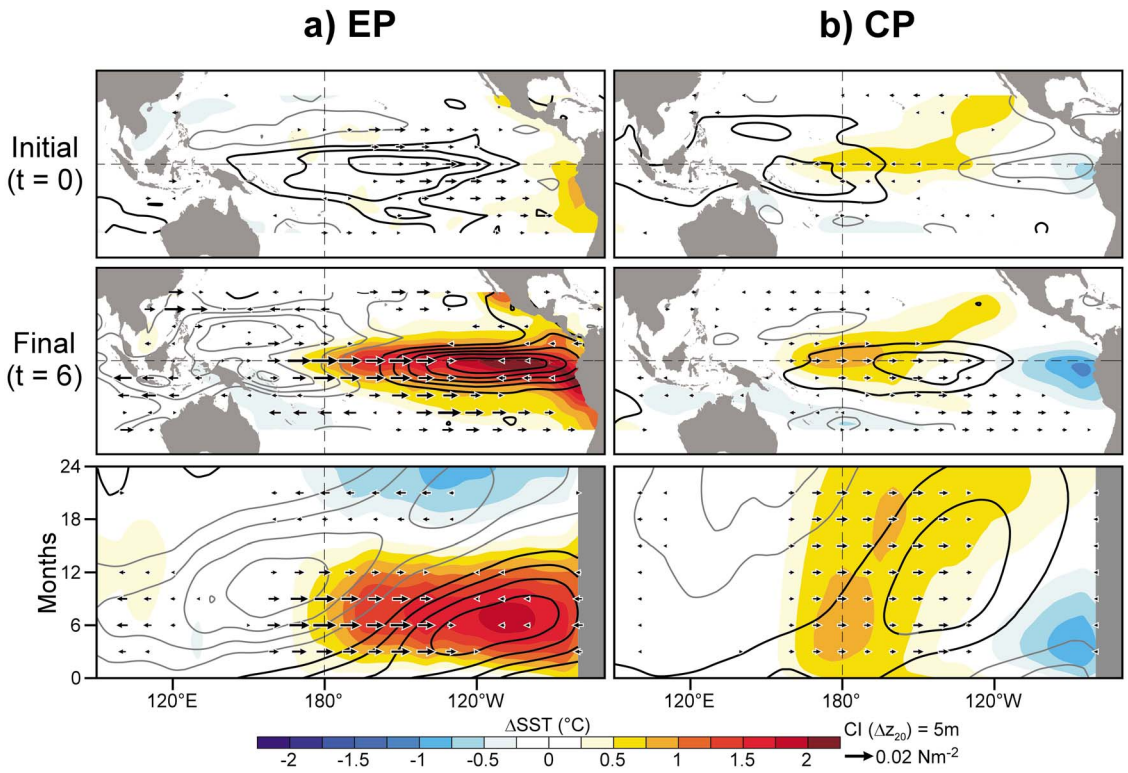

Figure 2. Leading patterns for SST anomaly amplification over a six-month interval (i.e., optimal structures), determined from a singular vector decomposition of the system propagator exp(6L) under the L2 norm (i.e., domain-mean square amplitude) of anomalous SST. (a) Evolution of the first pattern (which leads to an EP-type ENSO), shown as maps at (top) t = 0 and (middle) t = 6 months, and (bottom) as a time-longitude cross-section of the evolution along the equator. (b) Same as Figure 2a except the evolution of the second pattern (which leads to a CP-type ENSO). Anomalous SST is indicated by shading (contour interval 0.25 K), thermocline depth by contours (contour interval 5 m, where black is positive), and zonal wind stress by black vectors (scaled by the reference vector 0.02 Nm^{-2}, with values below 0.002 Nm^{-2} removed for clarity). Note that the opposite-signed patterns lead to cold events.

quite well with the observed *r*(Niño3, Niño4). Note that if Niño3 and Niño4 were instead each independently fitted with univariate red noises, their expected correlation would be zero.

[9] Second, in Figure 2 we show the two optimal structures leading to SST amplification over an interval of six months. (This interval is chosen as a compromise between 9 months, the time of peak growth for the leading optimal, and 4 months, the peak for the second optimal.) The leading optimal structure (Figure 2a) leads to the maximum possible amplification of rms SST anomaly within the entire tropical domain, and the second optimal structure (Figure 2b) is orthogonal to the leading one at both $t = 0$ and $t = 6$ months. The evolution of both is shown in the Hovmollers at the bottom of each column. The leading optimal structure evolves into an "EP-ENSO" event. It is quite similar to the optimal structure for growth over nine months discussed by NAS, who also used a diagnosis of the feedbacks within **L** to show how this structure's observed evolution is driven by both surface and thermocline interactions [see also *Neelin et al.*, 1998], with the zonally averaged thermocline anomaly decreasing to zero as the amplitude of the SST anomaly maximizes, and subsequent decay and sign change, as in the classic "recharge-discharge" mechanism [*Jin*, 1997]. In contrast, the second optimal structure (which has not been studied before) evolves into a "CP-ENSO" event with **L** initially driving growth through "non-local" interactions within SST (e.g., advection of SST anomalies; see Figure 4b of NAS). In particular, the initial equatorial heat content anomaly is near zero and there is no recharge-discharge mechanism, also suggested by some other studies of warm CP events [*Kao and Yu*, 2009; *Kug et al.*, 2009]. Thus, although the SST anomaly grows fairly weakly, the lack of the discharge mechanism also slows its decay, allowing the anomaly to persist relatively longer than does the EP ENSO. This evolution of the CP optimal is consistent with NAS who suggested that without thermocline-surface interactions, overall SST variability would be weaker but also more persistent, and shifted west towards the central Pacific. In its second year the CP optimal evolution weakens slightly but then strengthens to the east, behavior characteristic of the multi-year CP events, as the thermocline anomaly evolves so that its feedback on SSTs becomes more important, especially further east.

[10] The projection of observed anomalies on the initial optimal structures is compared to the projection of observed SST anomalies upon the corresponding predicted evolved structures 6 months later in Figure 3. The high linear cor-

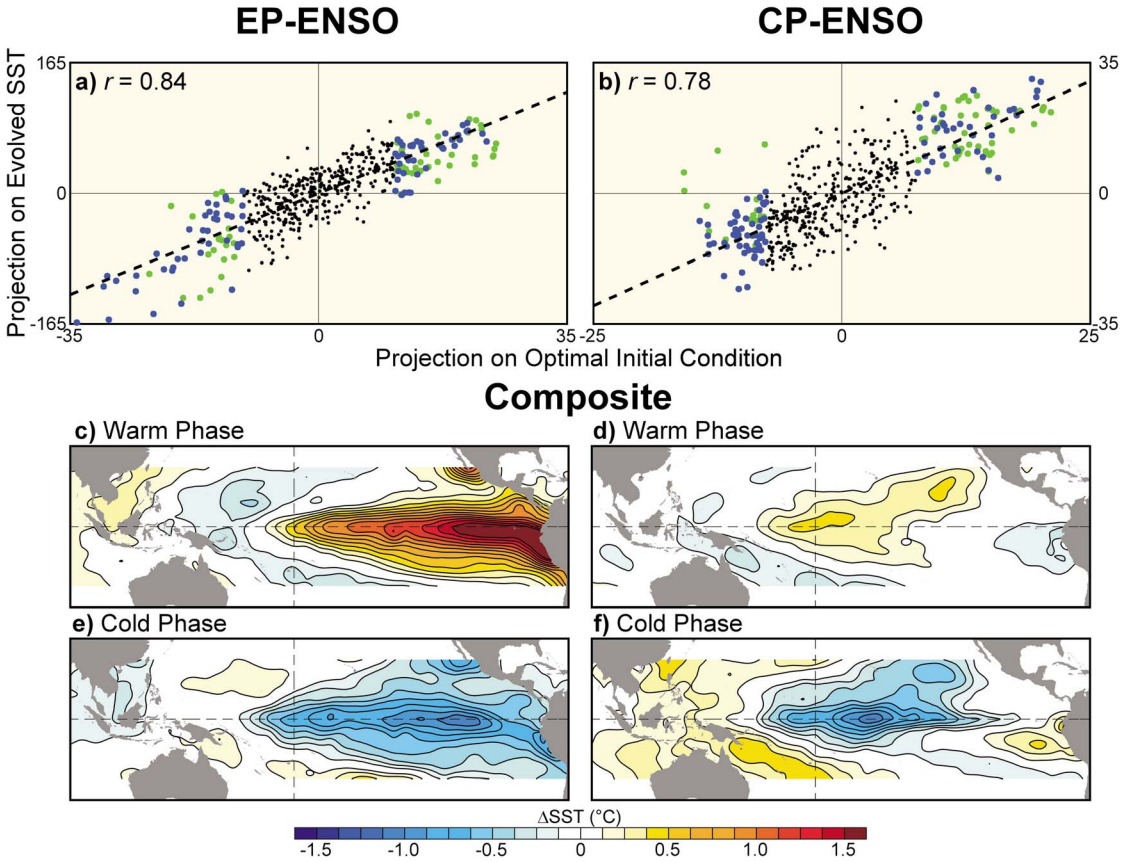

Figure 3. (top) Projection of observations upon the optimal initial condition for SST anomaly amplification over a six-month interval, versus the projection on the optimal evolved SST state 6 months later, for (a) the EP pattern and (b) the CP pattern. Note that the tropical SST growth factor for the EP pattern is almost 4 times greater than for the CP pattern. Blue dots indicate initial anomalies with large projection (magnitude greater than 1 standard deviation) on *either* the EP-ENSO *or* CP-ENSO optimal structure amplitudes, but not both; green dots indicate initial anomalies with large projection (over 1 standard deviation) on *both* optimal structures. (bottom) HadISST [*Rayner et al.*, 2003] SST composite anomalies constructed six months following the dates represented by the blue dots. Composites are constructed separately for (c and d) positive (warm phase) and (e and f) negative (cold phase) projection values. Anomalies with initially high projection on both optimal patterns (i.e., green dots) are excluded from the composites.

relation of these projections for each initial/evolved pair indicates that this *potential* optimal SST growth *does occur* as expected from multivariate red noise; that is, the case-to-case evolution of anomalies is well captured by (1), with the slopes of the least square lines matching the expected amplification factors, plus some remaining scatter due to noise. In contrast to earlier studies suggesting that CP events are warm phase only [e.g., *Kug et al.*, 2009], Figure 3b shows that CP-ENSO events of both signs occur (as by *Yu and Kim* [2011]), which is also seen in separate positive and negative composites constructed from SST anomalies six months following all dates on which either the EP-ENSO or CP-ENSO optimal structure amplitudes exceeded 1 standard deviation (blue dots in Figures 3a and 3b). The EP (CP) composite in Figures 3c and 3e (Figures 3d and 3f) is consistent with the expected six-month evolution of the leading (second) optimal pattern. Anomalies with initially high projection on both optimal patterns (indicated by green dots) evolve in a correspondingly mixed manner (not shown). Moreover, no trend exists in the time series of either the CP optimal or evolved pattern; the EP optimal and evolved pattern time series have weak trends that are not significant.

4. Variations of EP and CP Events Driven by Noise

[11] Given that multivariate red noise matches the observed interannual variability of both EP and CP events in the Tropics, we can now assess the potential range of EP and CP variability over multidecadal epochs, assuming no underlying change in either the dynamics or the overall statistics of noise. Using the DJF mean each year of the 24000-year integration we computed the same statistical measures as *Yeh et al.* [2009]: the simultaneous value of r(Niño3, Niño4), and the occurrence ratio of CP/EP El Niño (i.e., warm event only) defined as the ratio of CP-El Niño to EP-El Niño events, using Yeh et al.'s classifications noted in section 1. Results for the full integration are shown in Figure 4a, where both measures are determined from 30-yr long intervals centered 10 years apart. Ranges of values for the integration are summarized in Table 1 by determining 95% confidence bounds from the large number of samples,

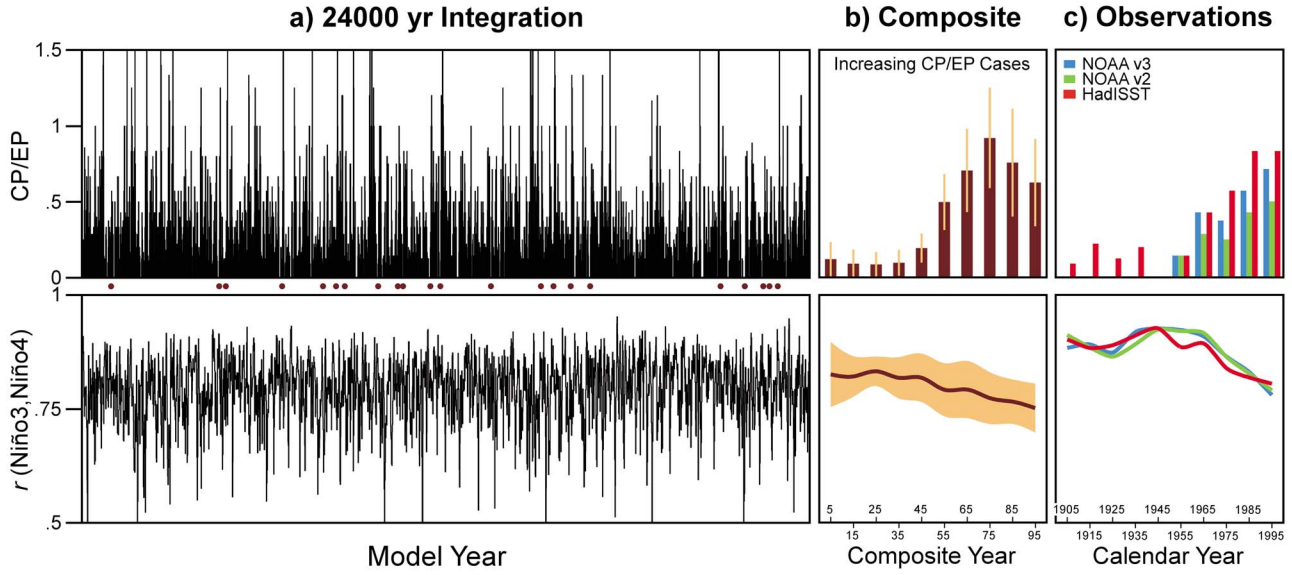

Figure 4. Measures of ENSO variations from multivariate red noise compared to observations. (top) CP/EP El Niño (i.e., warm event only) occurrence ratio and (bottom) *r* (Niño3, Niño4), for (a) the 24000 yr integration, (b) a composite over all the "increasing CP/EP cases" from the integration, with ±one standard deviation indicated by orange bars/shading, and (c) the SST datasets HadISST (red [*Rayner et al.*, 2003]), NOAA v2 (green [*Smith and Reynolds*, 2004]), and NOAA v3 (blue [*Smith et al.*, 2008]) for the years 1891–2010. In all cases the quantities are computed over 30-yr long intervals centered 10 years apart. Years on the abscissa represent the center of the 30-yr interval. The "increasing CP/EP cases," indicated by dots between Figures 4a (top) and 4a (bottom), are two adjacent 60-year segments for which the CP/EP ratio rises from below normal to above normal, and simultaneously *r*(Niño3, Niño4) decreases, from the first 60-yr segment to the second.

with sensitivity to the interval size determined by recomputing both measures using non-overlapping (i.e., adjacent) 10, 30, 50, or 100-yr intervals. As expected, shorter intervals show much greater variations in EP and CP events. In fact, it is possible to go up to 28 years between EP-El Niño events, and about one in seven 30-yr intervals have no CP-El Niño events. But even over centennial time scales long-term trends in ENSO characteristics are possible simply due to variations in noise. Moreover, any change in long-term mean now is a *residual* of the variability, not a driver of it; for example, for 30-yr means a two standard deviation decrease of EP events results in a deepening of the equatorial thermocline of ~6 m in the central Pacific. These results suggest that even several decades of data may be insufficient to gain an adequate picture of potential externally forced trends in CP/EP variability.

[12] For comparison, the same measures determined from three different SST datasets for the years 1891–2010 are shown in Figure 4c, where again (now due to limited data) the 30-yr intervals have 10-yr overlaps. (Note that for both NOAA datasets, there are no CP events prior to the 1941–1970 interval.) Clearly, the potential range in both measures is larger than appears in the SST datasets, even when we repeat these calculations using nonoverlapping 10-yr time intervals (not shown). Of course, the frequency of CP-El Niño occurrence before 1960 is more uncertain due to the lack of long-term SST observations, especially over the central and eastern tropical Pacific Ocean [*Deser et al.*, 2010; *Giese et al.*, 2010], but additional earlier CP events would only decrease the displayed 20th century range. Moreover, a number of 120-yr long segments in the integration mimic the observational record. For example, we define "increasing CP/EP cases" in the integration as two adjacent 60-year segments for which the CP/EP ratio rises from below normal to above normal, and simultaneously *r*(Niño3, Niño4) decreases, from the first 60-yr segment to the second. Figure 4b shows that both measures averaged over only these 120-yr segments correspond quite well to Figure 4c.

5. Concluding Remarks

[13] Since multivariate red noise determined from observations provides an excellent baseline for the statistics of

Table 1. Sensitivity of Results to Interval Length[a]

Averaging Interval (yrs)	*r*(Niño3,Niño4)	Change in *r*(Niño3,Niño4), Consecutive Intervals	CP/EP Ratio	Change in CP/EP Ratio, Consecutive Intervals	% of Intervals Without CP Events
10	0.42–0.96	0.44	0–∞	∞	50
30	0.63–0.91	0.20	0–1.2	0.96	14
30 (10-yr overlap)	0.63–0.91	0.13	0–1.2	0.55	14
50	0.67–0.88	0.15	0–0.88	0.64	3.4
100	0.71–0.86	0.11	0.1–0.62	0.44	0.3

[a]First four columns: 95% confidence bounds determined from computing *r* and CP/EP, using different interval lengths, from a 24000 yr forward integration of (1). Last column: the total fraction of intervals that had no CP events.

observed tropical seasonal anomaly evolution, and particularly differentiates between CP and EP ENSO events, it serves as a useful null hypothesis against which possible changes in the nature of ENSO can be tested. In this case, all past variations in CP and EP ENSO events, at least as determined from current SST gridded datasets, as well as projected changes based on the SRES A1B scenario in the IPCC AR4 models (cf. Figure 3 of *Yeh et al.* [2009] to Figure 4 of this study), appear to be less than may be expected from natural random variability. Note that these results assume statistical stationarity; that is, large multidecadal changes in relative CP and EP ENSO occurrence are consistent with fixed statistics of the 1959–2000 period, with no "base state" change. Also, there was no trend mode (either temporal or spatial) within the CP optimal pattern. Obviously, some variation in these results is likely since **L** is only an approximation of the underlying **L** that would be determined from a longer period of data. The key point is that we are restricted not by an accounting of CP and EP events that have occurred in the past forty years but rather by the *average simultaneous and 3-month lagged relationships* between the variables and locations represented in our chosen state vector, which allow for the possibility of EP and CP events that are initiated and evolve in a manner consistent with these statistics but have not (yet) occurred.

[14] While CP and EP ENSOs may be randomly initiated, this study does suggest that their observed differences represent real dynamical differences in which the dominant physical processes depend on initial conditions, leading to CP ENSOs that may amplify less but also persist more than EP ENSOs. Of course, generally climate anomalies will not exactly project on either of the two optimal structures shown in Figure 2. Rather, since these structures are orthogonal, an anomaly that is some combination of these two would evolve as a linear combination (plus additional noise subsequent to the initial time). Consequently, many additional "flavors" of ENSO are possible; for example, adding equal amounts of the two initial patterns would lead to a suboptimal but more persistent ENSO. Given the strong relationships between initial and evolved patterns in Figure 3, these ENSO flavors and their global impacts should be predictable.

[15] It remains possible that anthropogenic forcing might drive a change in the dynamics and hence a change in ENSO as suggested by *Yeh et al.* [2009], but that this change is too small to be significant in the face of short data sets and far smaller model ensembles than are needed to discern it from natural variability [e.g., *Coelho and Goddard*, 2009; *Solomon and Newman*, 2011; *Deser et al.*, 2011]. Or anthropogenic effects might drive changes in dominant noise spatial structures rather than in the base state dynamics, which could still change ENSO characteristics. It may be some years, however, before we can determine from data if this is likely.

[16] **Acknowledgments.** The authors thank an anonymous reviewer and N. Schneider for helpful comments. This work was partially supported by the NOAA OAR CVP Program.

[17] The Editor thanks the two anonymous reviewers for their assistance in evaluating this paper.

References

Alexander, M. A., et al. (2002), The atmospheric bridge: the influence of ENSO teleconnections on air-sea interaction over the global oceans, *J. Clim.*, *15*, 2205–2231, doi:10.1175/1520-0442(2002)015<2205:TABTIO>2.0.CO;2.

Ashok, K., S. K. Behera, S. A. Rao, H. Weng, and T. Yamagata (2007), El Niño Modoki and its possible teleconnection, *J. Geophys. Res.*, *112*, C11007, doi:10.1029/2006JC003798.

Carton, J. A., and B. S. Giese (2008), A reanalysis of ocean climate using Simple Ocean Data Assimilation (SODA), *Mon. Weather Rev.*, *136*, 2999–3017, doi:10.1175/2007MWR1978.1.

Coelho, C. A. S., and L. Goddard (2009), El Niño-induced tropical droughts in climate change projections, *J. Clim.*, *22*, 6456–6476, doi:10.1175/2009JCLI3185.1.

Deser, C., A. S. Phillips, and M. A. Alexander (2010), Twentieth century tropical sea surface temperature trends revisited, *Geophys. Res. Lett.*, *37*, L10701, doi:10.1029/2010GL043321.

Deser, C., A. S. Phillips, V. Bourdette, and H. Teng (2011), Uncertainty in climate change projections: The role of internal variability, *Clim. Dyn.*, doi:10.1007/s00382-010-0977-x.

Di Lorenzo, E., et al. (2010), Central Pacific El Niño and decadal climate change in the North Pacific, *Nat. Geosci.*, *3*, 762–765.doi:10.1038/ngeo984

Farrell, B. (1988), Optimal excitation of neutral Rossby waves, *J. Atmos. Sci.*, *45*, 163–172, doi:10.1175/1520-0469(1988)045<0163:OEONRW>2.0.CO;2.

Giese, B. S., et al. (2010), The 1918/1919 El Niño, *Bull. Am. Meteorol. Soc.*, *91*, 177–183, doi:10.1175/2009BAMS2903.1.

Guilyardi, E., et al. (2009), Understanding El Niño in ocean-atmosphere general circulation models: Progress and challenges, *Bull. Am. Meteorol. Soc.*, *90*, 325–340, doi:10.1175/2008BAMS2387.1.

Hasselmann, K. (1976), Stochastic climate models. Part I. Theory, *Tellus*, *28*, 473–485, doi:10.1111/j.2153-3490.1976.tb00696.x.

Jin, F.-F. (1997), An equatorial ocean recharge paradigm for ENSO. Part I: Conceptual model, *J. Atmos. Sci.*, *54*, 811–829, doi:10.1175/1520-0469(1997)054<0811:AEORPF>2.0.CO;2.

Kalnay, E., et al. (1996), The NCEP/NCAR 40-year reanalysis project, *Bull. Am. Meteorol. Soc.*, *77*, 437–471, doi:10.1175/1520-0477(1996)077<0437:TNYRP>2.0.CO;2.

Kao, H.-Y., and J.-Y. Yu (2009), Contrasting eastern-Pacific and central-Pacific types of ENSO, *J. Clim.*, *22*, 615–632, doi:10.1175/2008JCLI2309.1.

Kim, H. M., P. J. Webster, and J. A. Curry (2009), Impact of shifting patterns of Pacific Ocean warming events on North Atlantic tropical cyclones, *Science*, *325*, 77–80, doi:10.1126/science.1174062.

Kug, J.-S., F.-F. Jin, and S.-I. An (2009), Two types of El Niño events: Cold tongue El Niño and warm pool El Niño, *J. Clim.*, *22*, 1499–1515, doi:10.1175/2008JCLI2624.1.

Lee, T., and M. J. McPhaden (2010), Increasing intensity of El Niño in the central-equatorial Pacific, *Geophys. Res. Lett.*, *37*, L14603, doi:10.1029/2010GL044007.

Mo, K. C. (2010), Interdecadal modulation of the impact of ENSO on precipitation and temperature over the United States, *J. Clim.*, *23*, 3639–3656, doi:10.1175/2010JCLI3553.1.

Moore, A. M., and R. Kleeman (1999), The nonnormal nature of El Niño and intraseasonal variability, *J. Clim.*, *12*, 2965–2982, doi:10.1175/1520-0442(1999)012<2965:TNNOEN>2.0.CO;2.

Neelin, J. D., D. S. Battisti, A. C. Hirst, F.-F. Jin, Y. Wakata, T. Yamagata, and S. E. Zebiak (1998), ENSO theory, *J. Geophys. Res.*, *103*, 14,261–14,290, doi:10.1029/97JC03424.

Newman, M. (2007), Interannual to decadal predictability of tropical and North Pacific sea surface temperatures, *J. Clim.*, *20*, 2333–2356, doi:10.1175/JCLI4165.1.

Newman, M., P. D. Sardeshmukh, and C. Penland (2009), How important is air-sea coupling in ENSO and MJO evolution?, *J. Clim.*, *22*, 2958–2977, doi:10.1175/2008JCLI2659.1.

Newman, M., M. A. Alexander, and J. D. Scott (2011), An empirical model of tropical ocean dynamics, *Clim. Dyn.*, doi:10.1007/s00382-011-1034-0.

Penland, C., and P. D. Sardeshmukh (1995), The optimal growth of tropical sea surface temperature anomalies, *J. Clim.*, *8*, 1999–2024, doi:10.1175/1520-0442(1995)008<1999:TOGOTS>2.0.CO;2.

Rayner, N. A., D. E. Parker, E. B. Horton, C. K. Folland, L. V. Alexander, D. P. Rowell, E. C. Kent, and A. Kaplan (2003), Global analyses of sea surface temperature, sea ice, and night marine air temperature since the late nineteenth century, *J. Geophys. Res.*, *108*(D14), 4407, doi:10.1029/2002JD002670.

Rudnick, D. L., and R. E. Davis (2003), Red noise and regime shifts, *Deep Sea Res., Part I*, *50*, 691–699, doi:10.1016/S0967-0637(03)00053-0.

Smith, T. M., and R. W. Reynolds (2004), Improved extended reconstruction of SST (1854–1997), *J. Clim.*, *17*, 2466–2477, doi:10.1175/1520-0442(2004)017<2466:IEROS>2.0.CO;2.

Smith, T. M., R. W. Reynolds, T. C. Peterson, and J. Lawrimore (2008), Improvements to NOAA's Historical Merged Land-Ocean Surface Temperature Analysis (1880–2006), *J. Clim.*, *21*, 2283–2296, doi:10.1175/2007JCLI2100.1.

Solomon, A., and M. Newman (2011), Decadal predictability of tropical Indo-Pacific Ocean temperature trends due to anthropogenic forcing in a coupled climate model, *Geophys. Res. Lett.*, *38*, L02703, doi:10.1029/2010GL045978.

Trenberth, K. E., and D. P. Stepaniak (2001), Indices of El Niño evolution, *J. Clim.*, *14*, 1697–1701, doi:10.1175/1520-0442(2001)014<1697:LIOENO>2.0.CO;2.

Wunsch, C. (1999), The interpretation of short climate records, with comments on the North Atlantic and Southern oscillations, *Bull. Am. Meteorol. Soc.*, *80*, 245–255, doi:10.1175/1520-0477(1999)080<0245:TIOSCR>2.0.CO;2.

Yeh, S.-W., et al. (2009), El Niño in a changing climate, *Nature*, *461*, 511–514, doi:10.1038/nature08316.

Yeh, S.-W., B. P. Kirtman, J.-S. Kug, W. Park, and M. Latif (2011), Natural variability of the central Pacific El Niño event on multi-centennial timescales, *Geophys. Res. Lett.*, *38*, L02704, doi:10.1029/2010GL045886.

Yu, J.-Y., and S. T. Kim (2010), Identification of central-Pacific and eastern-Pacific types of ENSO in CMIP3 models, *Geophys. Res. Lett.*, *37*, L15705, doi:10.1029/2010GL044082.

Yu, J.-Y., and S. T. Kim (2011), Relationships between extratropical sea level pressure variations and the central Pacific and eastern Pacific types of ENSO, *J. Clim.*, *24*, 708–720, doi:10.1175/2010JCLI3688.1.

M. A. Alexander and M. Newman, Physical Sciences Division, Earth System Research Laboratory, NOAA, 325 Broadway, Boulder, CO 80309, USA. (matt.newman@noaa.gov)

S.-I. Shin, College of Marine Science, University of South Florida, 140 7th Ave. S., St. Petersburg, FL 33701, USA.